SUPERSHEAR CRACK PROPAGATION IN SNOW SLAB AVALANCHE RELEASE: NEW INSIGHTS FROM NUMERICAL SIMULATIONS AND FIELD MEASUREMENTS

Grégoire Bobillier[1,2,*], Bertil Trottet[3], Bastian Bergfeld[1], Ron Simenhois[4], Alec van Herwijnen[1], Jürg Schweizer[1], Johan Gaume[1,2,5]

[1] WSL Institute for Snow and Avalanche Research SLF, Davos, Switzerland

[2] Climate Change, Extremes, and Natural Hazards in Alpine Regions Research Center CERC, Davos, Switzerland

[3] École Polytechnique Fédérale de Lausanne, Switzerland

[4] Colorado Avalanche Information Center, Boulder, CO, USA.

[5] Institute for Geotechnical Engineering, ETH Zurich, Switzerland

ABSTRACT

The release process of dry-snow slab avalanches begins with a localized failure within a porous, weak snow layer that lies beneath a cohesive slab. Subsequently, rapid crack propagation may occur within the weak layer, eventually leading to a tensile fracture across the slab, resulting if the slope is steep enough, to its detachment and sliding. The dynamics of crack propagation is believed to influence the size of the release area. However, the relationship between crack propagation dynamics and avalanche size remains incompletely understood. Notably, crack propagation speeds estimated from avalanche video analysis are almost one order of magnitude larger than speeds typically measured in field experiments. To shed more light on this discrepancy and avalanche release processes, we used discrete (DEM: discrete element method) and continuum (MPM: material point method) numerical methods to simulate the so-called propagation saw test (PST). On low angle terrain, our models showed that the weak layer fails mainly due to a compressive stress peak at the crack tip induced by weak layer collapse and the resulting slab bending. On steep slopes, we observed the emergence of a supershear crack propagation regime: the crack speed becomes higher than the slab shear wave speed. This transition occurs if the crack propagates over a distance larger than the super-critical crack length (approximately 5 m). Above the super-critical crack length, the fracture is mainly driven by the slope-parallel gravitational pull of the slab (tension) and, thus, shear stresses in the weak layer. These findings represent an essential additional piece in the dry-snow slab avalanche formation puzzle.

KEYWORDS: supershear crack propagation, numerical modeling, dry-snow slab avalanche release.

1. INTRODUCTION

Forecasting the avalanche danger is vital and relies on a solid comprehension of avalanche release processes. Among the various types of avalanches, accidents mainly arise from dry-snow slab avalanches. Dry-snow slab avalanches release is a multi-scale process that requires the presence of a highly porous weak snow layer buried beneath a cohesive snow slab. It starts with the formation of a localized failure within the weak layer induced by a perturbation, e.g. an additional load such as a skier. It may then lead to the formation of a crack which may rapidly propagate within the weak layer across the slope. During the propagation process, the slab can eventually fracture and detach if the slope angle is greater than the friction angle of the weak layer (approx. 30°; McClung, 1979; Schweizer et al., 2003; van Herwijnen and Heierli, 2009).

During the last two decades, our understanding of slab avalanche formation has greatly improved, in particular through the development of a fracture mechanical field test: the propagation saw test (PST; Gauthier and Jamieson, 2006; Sigrist and Schweizer, 2007; van Herwijnen and Jamieson, 2005). The PST consists of an isolated snow column containing a pre-identified weak layer. A crack is manually initiated in the weak layer with a snow saw until a critical crack length is reached, after which crack propagation is self-sustained without additional loading. Using a high-resolution and high-speed camera to capture the PST side wall deformation enables us to analyze the mechanical behavior of the different snowpack layers, such as slab deformation and weak layer structural collapse during the initiation and the dynamical crack propagation. Furthermore, several analytical and numerical PST models based on fracture and/or continuum mechanics have been developed to investigate crack propagation behavior and provide additional insights into the mechanics involved (Benedetti et al., 2019; Chiaia et al., 2008; Gaume et al., 2013; Gaume et al., 2018; Gaume et al., 2015; Gaume et al., 2017; Rosendahl and Weissgraeber, 2020a; Rosendahl and Weissgraeber, 2020b).

The dynamics of crack propagation are believed to influence the extent of the release area and, consequently, the avalanche size. Recognizing this, the PST has been increasingly used to investigate and explore the complex driving mechanisms governing the crack propagation dynamics (Bergfeld et al., 2022; Bergfeld et al., 2023; Bobillier et al., 2021; Gaume et al., 2018; Trottet et al., 2022). In recent studies by Bobillier (2022) and by Trottet et al. (2022) emergence of a steady-state crack propagation regime was highlighted using discrete (discrete element method, DEM) and continuum (material point method, MPM) numerical methods, respectively. On flat terrain, the weak layer fractures mostly due to a compressive stress peak at the crack tip induced by the bending of the slab and weak layer collapse. Consequently, the speed of crack propagation is bounded by the corresponding Rayleigh wave speed. On steep slopes, a supershear crack propagation regime may emerge; the crack speed becomes higher than the slab shear wave speed. This transition occurs if the crack propagates over a distance larger than the so-called super-critical crack length (approximately 5 m). Beyond this length, the fracture is mainly driven by the slope-parallel gravitational pull of the slab (tension) and, thus, shear stresses in the weak layer.

We aim to describe the processes involved during the two steady-state regimes of weak layer crack propagation: sub-Rayleigh and supershear. To this end, we performed numerical simulations (continuum and discrete numerical methods) and analyzed field measurements. We studied weak layer crack propagation dynamics during propagation saw tests (PST) and full-scale avalanches using high-speed videos of PST experiments and a high-quality avalanche movie. To simulate propagation saw tests, we employed both the discrete element method and the material point method.

2. DATA AND METHODS
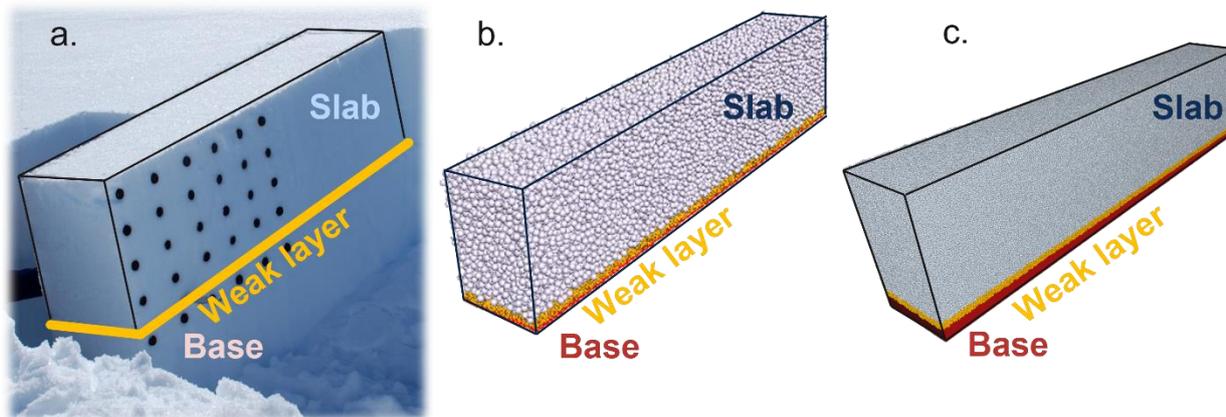
Figure 1: (a) Experimental propagation saw test (PST; photo: J. Schweizer). The black dots are markers used to measure slab deformation (particle tracking). (b) Discrete element method PST simulation, length 2 meters. (c) Material point method PST simulation.

Propagation saw test (PST)

The propagation saw test (PST) involves isolating a snow column with a pre-identified weak layer. A crack is manually created, with a saw, in the weak layer until it reaches the so-called critical length (a_c). Once this critical length is reached, crack propagation becomes self-sustained without requiring additional loading or manually expanding the crack. Over the last decades, the PST has been used to better understand the mechanisms driving the onset and the crack propagation dynamics (e.g., van Herwijnen et al., 2010). Particle tracking velocimetry (PTV) and/or digital image correlation (DIC) techniques were applied to measure slab deformation and derive crack propagation speed. Recently, this fracture mechanical field test has been extended to study dynamic crack propagation behavior over long distances (Bergfeld et al., 2022).

Discrete element method (DEM)

We developed a three-dimensional DEM model to simulate the PST behavior. Initially introduced by Cundall and Strack (1979), DEM is a numerical tool including numerous discrete interacting particles, commonly used to study large deformations in granular-like assemblies. Here, we use the commercial software PFC3D (v5) developed by Itasca. The simulated PSTs consist of three layers: a rigid basal layer, a transversely isotropic weak layer, similar to layers of surface hoar or facets, and a dense and uniform slab layer. The weak layer was created using cohesive ballistic deposition, resulting in a porosity of 80 % and a thickness (h) of 0.02 m. The slab layer was generated by cohesionless ballistic deposition with a porosity of 45 % and a thickness (H) of 0.4 m. We employed the parallel-bond contact model (PBM) for each layer to model particle interactions. The PBM enables elastic interactions between the

particles and if required, binding particles. The mechanical parameters include contact elastic modulus (E), Poisson's ratio (ν, restitution coefficient (e), friction coefficient (μ) and the bond strength (σ_c). Elastic modulus and strength have been modified for slab and weak layer in a range based on literature values (Mellor, 1975; Shapiro et al., 1997; Srivastava et al., 2016; van Herwijnen et al., 2016). We applied the Cundall-type numerical damping (e_u) for the weak layer particles to maintain the system's stability. No numerical damping was used for the slab particles to preserve slab elastic wave speed. During PST, the crack propagation speed is calculated from the difference in weak layer failure tip position at each time step ($c_{wl} = \Delta x / \Delta t$). For an in-depth description of the DEM-PST model readers are referred to Bobillier et al. (2021).

Material point method (MPM)

We developed a MPM model to simulate the PST behavior. The MPM is a hybrid Lagrangian–Eulerian particles-based numerical method, where Lagrangian particles track history-dependent variables like position, velocity, and deformation gradient, and an Eulerian grid enables the computation of spatial gradients for these quantities and is used to solve the equation of motion. The transfer of information between the grid and particles is achieved through an interpolation scheme based on quadratic B-splines and a FLIP/PIC algorithm. The slab is considered elastic and the weak layer is simulated using a modified cam clay yield surface with a hardening/softening model that allows for volumetric collapse (Gaume et al., 2018). The numerical set-up consists of a PST shape with a bilayer system composed of a cohesive elastic slab ($H = 0.5$ m) and an elastoplastic weak layer ($h = 0.125$ m). The thickness of the weak layer was chosen in the higher range of measured values in full propagation PST experiments (typically between 0.02 and 0.30 m thick). To initiate crack propagation, a virtual saw is used to initiate a crack in the weak layer. Once the critical crack length (a_c) is reached, the crack starts to propagate spontaneously. We conducted 2D simulations of PSTs with lengths ranging from 25 to 140 m to ensure a steady crack propagation regime across all simulations. During propagation, the crack speed is calculated from the difference in stress tip position at each time step ($c_{wl} = \Delta x / \Delta t$). The particles at the bottom of the weak layer were fixed in their positions. The complete constitutive models, as well as the slab and the weak layer parameter definition, are described Trottet et al. (2022).

Avalanche video sequences processing

Estimating crack speeds from avalanche videos involves detecting significant changes in pixel intensity caused by snow surface movement associated with weak layer fracture. This method comprises three steps:

1. Video stabilization

2. Tracking snow surface movement by detecting small changes in snow reflection

3. Estimating crack speed using motion segmentation between consecutive video frames

In the first step, the video is converted to grayscale, and an optical flow algorithm by Lucas and Kanade (1981) is used to stabilize the videos. The second step utilizes the principles of Eulerian video magnification (Wu et al., 2012) to detect small pixel intensity changes at the snow surface. Finally, pixel intensity is compared with the first temporal derivative to identify significant changes in pixel intensity at various locations. This technique captures the slab motion induced by crack propagation within the weak snow layer below, allowing estimation of crack propagation speed. More details about the method can be found in Simenhois et al. (2023).

3. RESULTS

Crack propagation regimes

We analyzed the crack propagation speed from two different numerical methods (DEM and MPM, Figure 2a,b) and from field measurements (Figure 2c). We used data from Bobillier et al. (2023) who present 79 flat and six titled DEM-PST simulations (Figure 2a). For the MPM simulations, we rely on data from Trottet et al. (2022) who describe 48 flat MPM-PST simulations, 191 titled MPM-PST simulations, seven flat field PSTs, nine short tilted field PSTs. For the full-scale avalanche video analysis, we present results from six cross-slope speed, and five down-slope speed measurements (Figure 2b, c).

The numerical PSTs on flat terrain, short field PSTs, and cross-slope propagation exhibited normalized speeds (normalized by the slab shear wave speed) below one, indicating a sub-Rayleigh propagation regime (Figure 2). In contrast, titled numerical PSTs and down-slope propagation showed normalized speeds above 1 and concentrated around 1.6 times the slab shear wave speed (Figure 2). We interpret this type of propagation regime as *supershear*, in analogy to supershear fracture speeds observed in other materials and earthquakes.
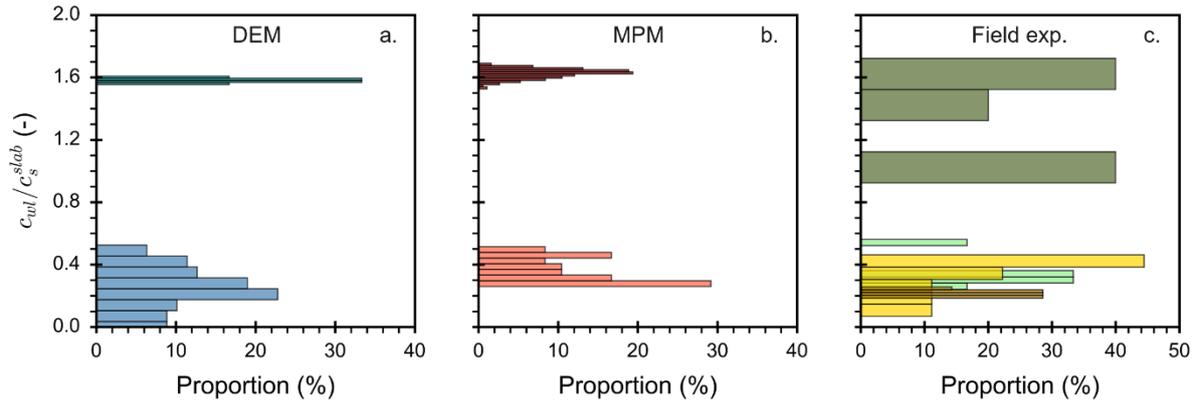
Figure 2: Frequency of crack propagation speed (normalized to slab shear wave speed). (a) DEM simulations (blue $\psi = 0°$, teal $\psi = 30 - 45°$). (b) MPM simulations (orange $\psi = 0 - 20°$, maroon $\psi = 25 - 50°$). (c) Field measurements, either extracted from short PSTs (dark yellow $\psi = 0°$, yellow $\psi = 37°$), or derived from avalanche video sequences (light green cross-slope and dark green down-slope crack propagation speeds).

4. DISCUSSION AND CONCLUSION

We present a comprehensive analysis of crack propagation behavior in weak snow layers. Our study employed field measurements in conjunction with two distinct numerical methods: DEM and MPM. By combining these approaches, we gained a multifaceted understanding of crack propagation dynamics. Through numerical simulations, we determined the crack speed based on stress tip position, as previously suggested by Bobillier et al. (2021). With the field data, we calculated crack propagation speed using digital image correlation (DIC) and Eulerian video detection (EVD) analysis, following the procedures described by Bergfeld et al. (2021) and Simenhois et al. (2023). These techniques allowed us to derive crack propagation speeds and provide new insights into the weak layer fracture behavior. Our analysis revealed the emergence of two distinct steady-state propagation regimes: sub-Raleigh and supershear.

The **sub-Rayleigh regime** is characterized by a crack propagation speed lower than the slab shear wave speed. Our observations on low angle terrain showed that the weak layer collapse and subsequent slab bending induced substantial concentration of compressive stresses (mode I), leading to self-sustained propagation. This behavior emphasizes the crucial role of weak layer microstructure and slab stiffness in governing crack initiation and propagation dynamics.

The **supershear regime** refers to crack propagation speeds exceeding the slab shear wave speed. On steep slopes, and when the crack extends beyond the so-called super-critical crack length (approximately 5 m), a change in fracture mode appears. Below this length, weak layer fracture mimics the stress state observed during the sub-Rayleigh regime. For propagation distances beyond the super-

critical crack length, fracture is driven by slope-parallel gravitational forces (tension) and shear stresses (mode II) within the weak layer.

The implications and significance of this new distinct pattern are profound, as it suggests that the propagation mechanism driving large slab avalanches would be in the supershear regime. This finding is crucial for estimating the size of slab avalanche releases, and, consequently, evaluating the avalanche danger. Our results suggest that weak layer mechanical properties and slab bending only have a minor influence on the dynamics of supershear propagation resulting in avalanche release. Hence, a simple shear model may in fact be sufficient to predict the size of large slab avalanches as has been originally proposed (e.g. McClung (1979)). This finding recently motivated the development of a depth-averaged MPM model where the weak layer is considered as a shear interface for the simulation of large avalanche release zones (Guillet et al., 2023). Our numerical simulations suggest that crack speed measurements from small-scale PSTs may not be representative of slope-scale crack speeds. Future research should include slope-scale experiments and simulations to investigate occurrence frequency and three-dimensional propagation patterns. A detailed analysis of the effect of slab fracture and topographic influences will help to refine estimates of avalanche release size based on snowpack properties and beyond the influence of terrain.

In conclusion, by integrating field measurements and advanced numerical methods, our study of weak layer crack propagation behavior has revealed two distinct crack propagation regimes: sub-Rayleigh and supershear. We established a new numerical framework that enhances our understanding of crack initiation, propagation, and the factors driving their behavior. These findings have implications for avalanche forecasting and risk assessment, offering a

refined approach to estimate avalanche release size based on the finding of supershear crack propagation. However, our study also shows the need for further research to consider three-dimensional crack propagation patterns, topography influences and slab fracture. While these findings represent an important step forward in our understanding of dry-snow slab avalanche formation, the link between crack propagation dynamics and the size of the avalanche release zone remains to be established.

REFERENCES

Benedetti, L., Gaume, J. and Fischer, J.T., 2019. A mechanically-based model of snow slab and weak layer fracture in the Propagation Saw Test. International Journal of Solids and Structures, 158: 1-20.

Bergfeld, B., van Herwijnen, A., Bobillier, G., Larose, E., Moreau, L., Trottet, B., Gaume, J., Cathomen, J., Dual, J. and Schweizer, J., 2022. Crack propagation speeds in weak snowpack layers. Journal of Glaciology, 68(269): 557-570.

Bergfeld, B., van Herwijnen, A., Bobillier, G., Rosendahl, P.L., Weißgraeber, P., Adam, V., Dual, J. and Schweizer, J., 2023. Temporal evolution of crack propagation characteristics in a weak snowpack layer: conditions of crack arrest and sustained propagation. Natural Hazards and Earth System Sciences, 23(1): 293-315.

Bergfeld, B., van Herwijnen, A., Reuter, B., Bobillier, G., Dual, J. and Schweizer, J., 2021. Dynamic crack propagation in weak snowpack layers: insights from high-resolution, high-speed photography. The Cryosphere, 15(7): 3539-3553.

Bobillier, G., 2022. Micro-mechanical modeling of dynamic crack propagation in snow slab avalanche release. Doctoral Thesis, ETH Zurich, Zurich, Switzerland, 146 pp.

Bobillier, G., Bergfeld, B., Dual, J., Gaume, J., van Herwijnen, A. and Schweizer, J., 2021. Micro-mechanical insights into the dynamics of crack propagation in snow fracture experiments. Scientific Reports, 11: 11711.

Bobillier, G., Bergfeld, B., Dual, J., Gaume, J., van Herwijnen, A. and Schweizer, J., 2023. Numerical investigation of crack propagation regimes in snow fracture experiments. Granular Matter: under review.

Chiaia, B.M., Cornetti, P. and Frigo, B., 2008. Triggering of dry snow slab avalanches: stress versus fracture mechanical approach. Cold Regions Science and Technology, 53(2): 170-178.

Cundall, P.A. and Strack, O.D.L., 1979. A discrete numerical model for granular assemblies. Geotechnique, 29(1): 47-65.

Gaume, J., Chambon, G., Eckert, N. and Naaim, M., 2013. Influence of weak-layer heterogeneity on snow slab avalanche release: application to the evaluation of avalanche release depths. Journal of Glaciology, 59(215): 423-437.

Gaume, J., Gast, T., Teran, J., van Herwijnen, A. and Jiang, C., 2018. Dynamic anticrack propagation in snow. Nature Communications, 9(1): 3047.

Gaume, J., van Herwijnen, A., Chambon, G., Birkeland, K.W. and Schweizer, J., 2015. Modeling of crack propagation in weak snowpack layers using the discrete element method. The Cryosphere, 9: 1915-1932.

Gaume, J., van Herwijnen, A., Chambon, G., Wever, N. and Schweizer, J., 2017. Snow fracture in relation to slab avalanche release: critical state for the onset of crack propagation. The Cryosphere, 11(1): 217-228.

Gauthier, D. and Jamieson, J.B., 2006. Towards a field test for fracture propagation propensity in weak snowpack layers. Journal of Glaciology, 52(176): 164-168.

Guillet, L., Blatny, L., Trottet, B. and Gaume, J., 2023. A depth-averaged material point method for shallow landslides: applications to snow slab avalanche release.

Lucas, B.D. and Kanade, T., 1981. An iterative image registration technique with an application to stereo vision, IJCAI'81: 7th international joint conference on Artificial intelligence, pp. 674-679.

McClung, D.M., 1979. Shear fracture precipitated by strain softening as a mechanism of dry slab avalanche release. Journal of Geophysical Research, 84(87): 3519-3526.

Mellor, M., 1975. A review of basic snow mechanics, Symposium at Grindelwald 1974 - Snow Mechanics, IAHS Publ., 114. International Association of Hydrological Sciences, Wallingford, Oxfordshire, U.K., pp. 251-291.

Rosendahl, P.L. and Weissgraeber, P., 2020a. Modeling snow slab avalanches caused by weak-layer failure - Part 1: Slabs on compliant and collapsible weak layers. The Cryosphere, 14(1): 115-130.

Rosendahl, P.L. and Weissgraeber, P., 2020b. Modeling snow slab avalanches caused by weak-layer failure - Part 2: Coupled mixed-mode criterion for skier-triggered anticracks. The Cryosphere, 14(1): 131-145.

Schweizer, J., Jamieson, J.B. and Schneebeli, M., 2003. Snow avalanche formation. Reviews of Geophysics, 41(4): 1016.

Shapiro, L.H., Johnson, J.B., Sturm, M. and Blaisdell, G.L., 1997. Snow mechanics - Review of the state of knowledge and applications. CRREL Report 97-3, US Army Cold Regions Research and Engineering Laboratory, Hanover, N.H., U.S.A.

Sigrist, C. and Schweizer, J., 2007. Critical energy release rates of weak snowpack layers determined in field experiments. Geophysical Research Letters, 34(3): L03502.

Simenhois, R., Birkeland, K.W., Gaume, J., van Herwijnen, A., Bergfeld, B., Trottet, B. and Greene, E., 2023. Using video detection of snow surface movements to estimate weak layer crack propagation speeds. Annals of Glaciology: 1-11.

Srivastava, P.K., Chandel, C., Mahajan, P. and Pankaj, P., 2016. Prediction of anisotropic elastic properties of snow from its microstructure. Cold Regions Science and Technology, 125: 85-100.

Trottet, B., Simenhois, R., Bobillier, G., Bergfeld, B., van Herwijnen, A., Jiang, C.F.F. and Gaume, J., 2022. Transition from sub-Rayleigh anticrack to supershear crack propagation in snow avalanches. Nature Physics, 18(9): 1094–1098.

van Herwijnen, A., Gaume, J., Bair, E.H., Reuter, B., Birkeland, K.W. and Schweizer, J., 2016. Estimating the effective elastic modulus and specific fracture energy of snowpack layers from field experiments. Journal of Glaciology, 62(236): 997-1007.

van Herwijnen, A. and Heierli, J., 2009. Measurement of crack-face friction in collapsed weak snow layers. Geophysical Research Letters, 36(23): L23502.

van Herwijnen, A. and Jamieson, B., 2005. High-speed photography of fractures in weak snowpack layers. Cold Regions Science and Technology, 43(1-2): 71-82.

van Herwijnen, A., Schweizer, J. and Heierli, J., 2010. Measurement of the deformation field associated with fracture propagation in weak snowpack layers. Journal of Geophysical Research, 115: F03042.

Wu, H.-Y., Rubinstein, M., Shih, E., Guttag, J., Durand, F. and Freeman, W., 2012. Eulerian video magnification for revealing subtle changes in the world. ACM transactions on graphics (TOG), 31(4): 1-8.